THE ASTROPHYSICAL JOURNAL, 489:170–174, 1997 November 1

VERY HIGH-ENERGY OBSERVATIONS OF PSR B1951+32

R. SRINIVASAN,[1] P. J. BOYLE,[2] J. H. BUCKLEY,[3] D. A. CARTER-LEWIS,[4] M. CATANESE,[4] M. F. CAWLEY,[5] E. COLOMBO,[3,6] D. J. FEGAN,[2] J. P. FINLEY,[1] J. A. GAIDOS,[1] J. BUSSONS GORDO,[2] A. M. HILLAS,[7] F. KRENNRICH,[4] R. C. LAMB,[8] R. W. LESSARD,[1] J. M. MCENERY,[2] P. MORIARTY,[9] J. QUINN,[2] H. J. ROSE,[7] F. W. SAMUELSON,[4] G. SEMBROSKI,[1] T. C. WEEKES,[3] C. WILSON,[1] AND J. ZWEERINK[4]

Received 1997 March 12; accepted 1997 June 11

ABSTRACT

PSR B1951+32 is a γ-ray pulsar detected by the *Energetic Gamma Ray Experiment Telescope* (EGRET) and identified with the 39.5 ms radio pulsar in the supernova remnant CTB 80. The pulsar energy spectrum is consistent with an unbroken power law with differential photon index of -1.8 ± 0.1 between 50 MeV and 10 GeV. The EGRET data shows no evidence for a spectral turnover. Here we report on the first observations of PSR B1951+32 beyond 30 GeV. The observations were carried out with the 10 m γ-ray telescope at the Whipple Observatory on Mount Hopkins, Arizona. In 8.1 hours of observation we find no evidence for steady or periodic emission from PSR B1951+32 above $\sim$260 GeV. Flux upper limits are derived and compared with model extrapolations from lower energies and the predictions of emission models.

Subject headings: gamma rays: observations — pulsars: individual (PSR B1951+32) — supernova remnants

1. INTRODUCTION

The pursuit of very high-energy (VHE) astrophysics has resulted in the discovery of five sources, of which three are associated with young spin-powered pulsars. Astronomy in the VHE range, i.e., $E \geq 100$ GeV, was given a new impetus after the launch of the *Energetic Gamma Ray Experiment Telescope* (EGRET) aboard the *Compton Gamma-Ray Observatory* (*CGRO*). The success of EGRET in the 30 MeV–30 GeV energy range suggests a candidate source list for follow-up VHE observations. To date, the only identified Galactic point sources seen by EGRET are six spin-powered pulsars, namely, Crab (PSR B0531+21), Vela (PSR B0833−45), Geminga (Bertsch et al. 1992), PSR B1706−44 (Thompson et al. 1992), PSR B1055−52 (Fierro et al. 1993), and PSR B1951+32 (Ramanamurthy et al. 1995). VHE emission has been detected from the direction of the Crab Nebula (Vacanti 1991), the Vela pulsar (Takanori 1996), and PSR B1706−44 (Kifune et al. 1995), but no evidence has been found for periodic emission at these energies in these experiments. Upper limits on periodic emission have been reported for the Crab pulsar (Gillanders et al. 1997).

The detection of VHE γ rays utilizes the Atmospheric Čerenkov technique (ACT), in which the Čerenkov radiation emitted by the electromagnetic cascade initiated by γ-ray or cosmic-ray primaries is detected by a ground-based telescope (Weekes 1996). Improved telescopes, focal plane detectors and data analysis techniques allow efficient discrimination of the γ rays from the cosmic-ray background. The energy range of the atmospheric Čerenkov imaging telescopes achieved to date extends beyond the EGRET detector, which has a sensitivity up to 30 GeV.

Currently, there are two principal models of high-energy pulsar emission based on the location of the particle acceleration regions. Outer gap models assume that particles are accelerated in the vacuum gaps in the outer magnetosphere and induce pair cascades through γ-γ pair production (Cheng, Ho, & Ruderman 1986; Romani & Yadigaroglu 1995). Polar cap models assume that particles are accelerated along open field lines near the neutron star by parallel electric fields and induce pair cascades by either curvature radiation (Daugherty & Harding 1982) or inverse-Compton radiation (Dermer & Sterner 1994). Outer gap models predict a higher flux, relative to polar cap models of pulsed VHE γ rays since in polar gap models VHE γ rays are absorbed by the strong magnetic field near the stellar surface. Measurement of a pulsed flux at VHE energies would discriminate between these models.

PSR B1951+32 was discovered as a 39.5 ms pulsar embedded in a radio synchrotron nebula (CTB 80) (Kulkarni et al. 1988). The rotational parameters of PSR B1951+32 ($P = 39.5$ ms, $\dot{P} \cong 5.85 \times 10^{-15}$ s s^{-1}) indicate a dynamic age of $\sim 10^5$ yr. The measured and derived parameters of PSR B1951+32 are displayed in Table 1. PSR B1951+32 has also been detected as a pulsating X-ray source (Safi-Harb et al. 1995) and as a high-energy γ-ray pulsar at $E \geq 100$ MeV at the radio period (Ramanamurthy et al. 1995). It can be inferred from the five pulsars seen in the MeV to GeV γ-ray region that longer period or older ($\sim 10^5$ yr) pulsars have a greater fraction of spin-down energy emitted as high-energy γ rays. With a luminosity of 1.4×10^{34} ergs s^{-1} at EGRET energies, PSR B1951+32 has an efficiency $\eta \sim 0.4\%$ of converting the rotational

[1] Department of Physics, Purdue University, West Lafayette, IN 47907-1396; radhika@purds1.physics.purdue.edu.
[2] Physics Department, University College, Dublin 4, Ireland.
[3] Whipple Observatory, Harvard-Smithsonian CfA, P.O. Box 97, Amado, AZ 85645-0097.
[4] Department of Physics and Astronomy, Iowa State University, Ames, IA 50011-3160.
[5] Physics Department, St. Patrick's College, Maynooth, County Kildare, Ireland.
[6] Present address: CONAE, Paseo Colon 751, Argentina.
[7] Department of Physics and Astronomy, University of Leeds, Leeds, LS2 9JT, Yorkshire, England, UK.
[8] Space Radiation Lab, California Institute of Technology, Pasadena, CA 91125.
[9] Regional Technical College, Galway, Ireland.

TABLE 1

PULSAR PARAMETERS

PSR	P (ms)	$\dot{P}$ (10^{-15} s s^{-1})	Distance (kpc)	$\mathrm{Log}_{10} B$ (G)	$\mathrm{Log}_{10} \dot{E}$ (ergs s^{-1})
B1951+32.....	39.53	5.8494	2.5	11.69	36.57

NOTE.—Data from Taylor et al. 1993.

energy loss of the pulsar into γ rays. (Ramanamurthy et al. 1995). The best-fit outer gap model of Zhang & Cheng (1997) suggests that PSR B1951+32 should emit detectable levels of TeV γ rays (Fig. 4). The multiwavelength spectrum of PSR B1951+32 (Fig. 3*b*) indicates a maximum power per decade at energies consistent with a few GeV and still rising at 10 GeV. These factors make PSR B1951+32 a good candidate for observations with the ACT above 100 GeV.

We report here on our search for steady and pulsed emission from PSR B1951+32 during the 1996 observing season. The format of the paper is the following: in § 2, we describe the observations; § 3 contains a description of the analysis technique and the results for steady and periodic emission. Finally, a discussion of the results is presented in § 4.

2. OBSERVATIONS

The observations of PSR B1951+32 reported here were acquired with the 10 m reflector located at the Whipple Observatory on Mount Hopkins in Arizona at an elevation 2.3 km. The camera, consisting of 109 photomultiplier tubes (PMT), is mounted in the focal plane of the reflector and records images of atmospheric Čerenkov radiation produced by electromagnetic cascades initiated by γ rays and cosmic rays (Cawley & Weekes 1995). Hereafter, *On* source observations refer to those where the putative source is at the center of the field of view. For *Off* source observations, the telescope tracks the same declination as the putative source but is offset in right ascension so that *On*/*Off* data sets cover the same elevation and azimuth regions. The *Off* source data check the systematics of the instrument and the *On*/*Off* observations are also used to estimate the background.

For a majority of the observations, data were taken in the *Tracking* mode where the reflector tracks the *On* source position and no data is taken *Off* source. The background for *Tracking* observations is estimated from events that do not appear to originate from the source direction. A subset of observations were acquired in the *On*/*Off* mode. A total of 14 *Tracking* runs and 4 *On*/*Off* pairs taken between 1996 May 13 and July 17 constitute the database for all subsequent discussion. The average elevation for the data set was $\sim 74°$ under good sky conditions. The total *On* source observing time is 8.1 hr. The radio position (J2000) of PSR B1951+32 ($\alpha = 19^{\mathrm{h}}52^{\mathrm{m}}58^{\mathrm{s}}.25$, $\delta = 32°52'40''.9$) (Taylor, Manchester, & Lyne 1993) was assumed for the subsequent timing analysis.

3. ANALYSIS AND RESULTS

3.1. *Standard Analysis*

The event selection criteria basically differentiate between the smaller, more elliptical images characteristic of γ rays from the broader more irregular shaped images produced by cosmic-ray primaries. The images recorded are parameterized in the form of an ellipse using a moment fitting algorithm (Hillas 1985). Optimization on the Crab Nebula data indicated that γ-ray images are associated with specific parameter domains.

The γ-hadron separation is based upon *shape* criteria and the point source excess is determined by the image orientation given by the *alpha* parameter. The *shape* cuts consist of selections based on the *width* (minor axis of the ellipse) and *length* (major axis of the ellipse) of the image. In addition, a selection criteria based upon the distance of the image centroid from the field center (*distance* parameter) was also applied. The lower *distance* cut discards circular images that provide no γ-hadron discrimination, while the higher *distance* cut eliminates truncated images (i.e., images not contained within the fiducial area of the camera). These selection criteria are collectively called *Supercuts* (Punch et al. 1991). Increased background caused by reduction in energy threshold requires a slight modification to *Supercuts*. Čerenkov signals from local muons tend to pass the *shape* cuts and hence it is required that only images with a minimum of the total integrated light in the event of ≥ 400 photoelectrons (p.e.) be accepted. This is referred to as the *size* parameter. Noise triggers were eliminated by requiring that there be three adjacent PMTs above the triggering threshold. A software trigger threshold is utilized that requires at least one PMT channel (*max1*) be above 100 p.e. and a second (*max2*) be above 80 p.e. These modified selection criteria are collectively called *Supercuts95* (Catanese et al. 1995). The γ rays originating from the point source, which is at the center of the field of view, will have their major axis pointed toward the center of the camera. The orientation angle *alpha* (α) is defined as the angle between the major axis of the ellipse and the line joining the centroid of the ellipse and the center of the camera. A point source detection is based on an excess seen in the α region between 0° and 15° referred to as the γ-ray domain. Events whose orientations are such that they are not from the direction of the source (i.e., between 20° and 65°, also referred to as the control region) are used in the estimation of the background level for *Tracking* observations.

Supercuts95 raises the effective energy threshold of the detector with its software trigger and *size* cuts. For sources such as the Crab Nebula, which have a spectrum extending to a few TeV, *Supercuts95* improves the sensitivity of the detector to its emission. PSR B1951+32, however, appears to have a steep spectrum at EGRET energies and since the pulsar spectrum is expected to cut off, it behooves us to reduce the threshold of our analysis to search for a lower energy signal. The dominant background at lower energies is due to muons whose images appear in the camera as arcs. Muon images tend to have a large value of the *length* parameter associated with small *size* (due to their low light level) and can be discriminated by a cut on their large *length*/*size* values. Hence, the selection criteria used *Supercuts95* on images with sizes larger than 400 p.e. and *Smallcuts* (Table 2) for images with sizes less than 400 p.e. The *Off* observations are used to determine the factor, called the *tracking ratio*, which converts the events in the control region of the *Tracking* mode observations to a background estimate in the γ-ray domain so that *tracking ratio* = sum (20°–65°)/sum (0°–15°). The *tracking ratio* obtained from events selected with *Supercuts95* only, is 3.82 ± 0.53. A slightly different estimate for this ratio of 3.17 ± 0.24 is obtained by using events selected with *Supercuts95* and *Smallcuts*.

TABLE 2

PARAMETER RANGES FOR SELECTING γ-RAY IMAGES

Parameter	*Supercuts95*	*Smallcuts*
Length (deg)	0.16–0.30	Unchanged
Width (deg)	0.073–0.15	Unchanged
Distance (deg)	0.51–1.1	Unchanged
Alpha (deg).....	<15	Unchanged
max1 (p.e.)	>100[a]	45–100
max2 (p.e.)	>80	45–80
Size (p.e.)	≥ 400	0–400
Length/size (deg/p.e.).....	Not used	$<7.5 \times 10^{-4}$

NOTE.—See text for parameter descriptions.

[a] 1 photoelectron (p.e.) is equivalent to 1 digital count (d.c.) (Biller et al. 1995).

The data set used to search for steady emission was a combination of both the *On/Off* and *Tracking* data sets (see Table 3). No steady emission is detected from PSR B1951+32 and 3 σ flux upper limits, including both the *Tracking* and *On/Off* data sets, are displayed in Table 5 below. The effective area for *Supercuts95*, which was used to calculate the upper limit, was taken as $A_{\rm eff} \sim 3.5 \times 10^8$ cm^2: the same area was used for the data set that resulted from a combination of *Supercuts95* and *Smallcuts*, although here there is more systematic uncertainty. The energy threshold was obtained from simulations and extrapolating the Crab Nebula γ-ray rate for each set of cuts used assuming a spectrum $\sim E^{-2.4}$.

3.2. *Periodic Analysis*

The arrival times of the Čerenkov events were registered by a GPS clock with an absolute resolution of 250 μs. An oscillator calibrated by GPS second marks was used to interpolate to a resolution of 0.1 μs. After an oscillator drift correction was applied, all arrival times were transformed to the solar system barycenter and folded to produce the phases, ϕ_j, of the events modulo the pulse period according to

$$\phi_j = \phi_0 + \nu(t_j - t_0) + \tfrac{1}{2}\dot{\nu}(t_j - t_0)^2 \,, \qquad (1)$$

where ν and $\dot{\nu}$ are the frequency and first frequency derivative, respectively. The ephemeris frequency parameters used were $\nu = 25.2963719901267$ s^{-1} and $\dot{\nu} = -3.73940 \times 10^{-12}$ s^{-2}, at the epoch $t_0 =$ JD 2450177.5 (Lyne 1996). This frequency was extrapolated 72 days to obtain a timing solution relevant to the epoch of observation. The data sets, however, were taken within the validity interval of the above ephemeris.

To check the Whipple Observatory timing systems an *optical* observation of the Crab pulsar was undertaken on 1996 December 2 (UT) using the 10 m reflector (Srinivasan 1997). The Crab pulsar was observed with an aperture on the central phototube and the voltages on all other tubes zeroed so that the 10 m γ-ray telescope operated as an optical telescope with a photometer at its focus. The phase analysis of the event arrival times yielded a clear detection of the optical Crab pulsar signal (Fig. 1), which is in phase with the radio and demonstrates the validity of the timing, data acquisition, and analysis software in the presence of a pulsed signal.

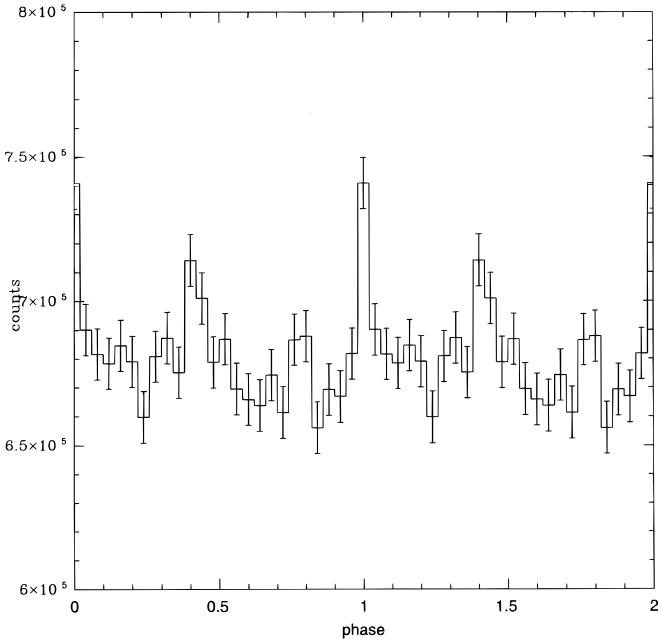

FIG. 1.—Observation of the *optical* Crab pulsar with the 10 m γ-ray telescope to determine the accuracy of the Whipple Observatory timing systems. The light curve shows a clear detection of the optical Crab pulsations. Phase 0.0 corresponds to the extrapolated arrival of the radio peak closest to the epoch of observation from the 1996 November 15 ephemeris.

The light curve that results from phase analysis of events selected by *Supercuts95* and *Smallcuts* selection criteria is displayed in Figure 2. No evidence of pulsed emission at the radio period exists. To calculate a pulsed flux upper limit we assumed the same pulse profile as seen at EGRET energies, i.e., with the phase range for the main pulse and secondary pulse as 0.12–0.22 and 0.48–0.74, respectively (Ramanamurthy et al. 1995), so that the number of photons in this region is taken as the source photons (N_{ON}). The sum of photons in bins excluding the aforementioned phase regions contributes to the background (N_{OFF}) so that $N_{ON} - \beta N_{OFF}$ corresponds to the total number of pulsed photons or excess in the pulsed regions. β is the ratio of the number of pulsed bins to the number of off pulse bins. This results in the sample displayed in Table 4, where $\sigma = (N_{ON} + \beta^2 N_{OFF})^{1/2}$.

The 3 σ upper limit results for pulsed emission displayed in Table 5 were calculated under the assumption that the pulse profile at VHE energies is aligned with the main and secondary pulse seen at EGRET energies.

TABLE 3

SELECTED EVENTS FOR STEADY EMISSION ANALYSIS

Selection	Source Events ($\alpha < 15°$)	Background Events ($\alpha < 15°$)	Excess	Significance
Supercuts95	292	254	38	1.16 σ
Smallcuts.....	618	672	-54	-1.10 σ
Supercuts95 + *Smallcuts*.....	910	926	-16	-0.24 σ

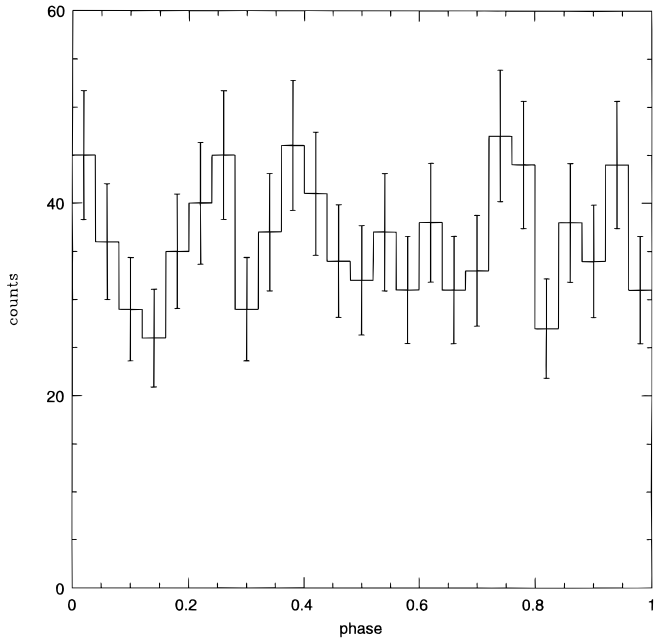

FIG. 2.—Light curve of PSR B1951+32 using events selected by the *Supercuts95* + *Smallcuts* selection criteria. Phase 0.0 corresponds to the extrapolated arrival of the radio peak closest to the epoch of observation.

4. DISCUSSION

PSR B1951+32 is surrounded by a compact nebula that gives a plerionic nature to the supernova remnant, CTB 80. Such plerions form when the relativistic wind from a pulsar is confined by a more slowly expanding shell of the surrounding supernova remnant. The prototypical example of a plerion, the Crab Nebula, was predicted as a source of TeV emission (Gould 1965). X-ray plerions are good candidates for VHE emission since the electrons responsible for nebular synchrotron X-rays should also create VHE γ rays via the inverse Compton (IC) process. Calculated synchrotron-self Compton (SSC) spectra provide a very good fit to the observed γ-ray spectrum of the Crab Nebula (De Jager et al. 1996). It is expected that for plerions, such as that associated with PSR B1951+32 where the density of nebular synchrotron photons is too low for SSC to take place, detectable VHE emission should be produced by the IC scattering of the 2.7 K cosmic microwave background by the same electrons radiating synchrotron X-ray photons (De Jager et al. 1995). Interpreting the unpulsed X-ray emission form CTB 80 as the synchrotron emission from a plerion, the estimated IC flux of more than 1 TeV is 6.6×10^{-13} TeV cm^{-2} s^{-1} TeV^{-1} (De Jager et al. 1995). This represents the lower limit on the IC flux since there can be other sources of soft photons in addition to the microwave background. The predicted flux depends on the assumptions made to derive the magnetic field of the plerion. Using the expression for the IC spectrum given in De Jager et al. (1995) the estimated flux of more than 370 GeV corresponds to 1.8×10^{-12} TeV cm^{-2} s^{-1} TeV^{-1}, which is below the steady emission flux upper limit reported here.

To model the pulsed high-energy spectrum, a function of the form

$$dN_\gamma/dE = KE^{-\Gamma}e^{(-E/E_0)} \quad (2)$$

was used where E is the photon energy, Γ is the photon spectral index and E_0 is the cutoff energy. This relation is expected to be valid if a cutoff is caused by magnetic pair production or synchrotron radiation of electrons with a certain maximum energy. The source spectrum in the EGRET energy range (50 MeV–10 GeV) is well represented by a power law with differential photon spectral index -1.8 ± 0.1 (Fierro 1995). The pulsed upper limit reported here is 2 orders of magnitude lower than the extrapolated EGRET power law. Equation (2) was used to extrapolate the EGRET spectrum to VHE energies constrained by the TeV upper limit reported here and indicates a cutoff energy of $E_0 \leq 75$ GeV for pulsed emission (Fig. 3*a*). The strength of the cutoff provides a good discriminant between the various pulsar emission models. The status of current observations and the derived cutoff discussed above indicates that the cutoff is beyond 10 GeV. In polar cap models this would indicate a sharp cutoff since the pair production optical depth increases exponentially with photon energy (Harding 1997). However, it is not possible to constrain the shape of the cutoff with the nondetection of pulsed TeV flux reported here.

The most relevant comparison of the Whipple upper limit with emission models is the outer gap model of Zhang & Cheng (see Fig. 4). This model includes the effect of geometry in the treatment of pulsed emission via a parameter $\alpha = r/r_L$, the radial distance to the synchrotron emitting region near the outer gap, r, as a function of the light

TABLE 4

SELECTED EVENTS FOR PERIODIC EMISSION ANALYSIS

Selection	Source Events[a] ($\alpha < 15°$)	Background Events[a] ($\alpha < 15°$)	Excess	Significance
Supercuts95	92	113 ± 8	-21	$-1.65\ \sigma$
Supercuts95 + *Smallcuts*	313	336 ± 14	-23	$-1.03\ \sigma$

[a] See text for details.

TABLE 5

INTEGRAL FLUX UPPER LIMITS

	Steady Emission (cm^{-2} s^{-1})	Periodic Emission (cm^{-2} s^{-1})	Threshold (GeV)
Supercuts95[a]	0.97×10^{-11}	3.7×10^{-12}	≥ 370
Supercuts95 + *Smallcuts*[a]	1.95×10^{-11}	6.7×10^{-12}	≥ 260

[a] See text for details.

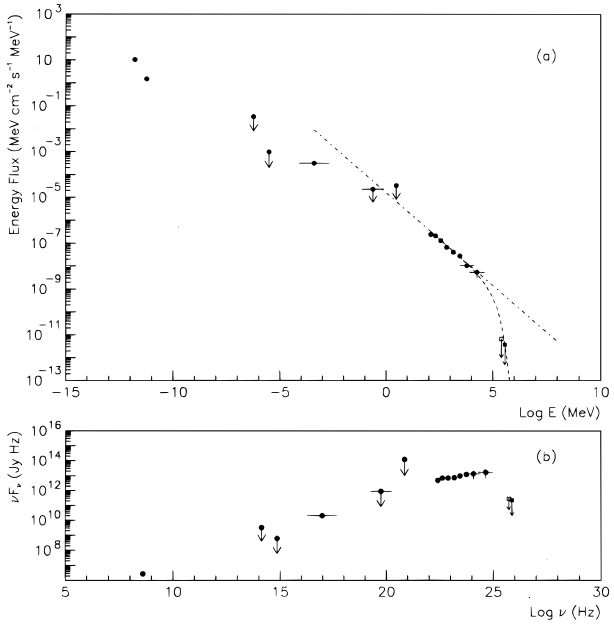

FIG. 3.—(*a*) Pulsed energy spectrum of PSR B1951+32 (Thompson 1996). The dot-dashed line represents the power-law fit to the EGRET points. The dashed curve represents eq. (2) with a cutoff energy $E_0 = 75$ GeV. The Whipple upper limits for pulsed emission are indicated by a filled square at a threshold of 370 GeV and an open square at a threshold of 260 GeV. (*b*) Pulsed spectral energy distribution of PSR B1951+32. The Whipple upper limits for pulsed emission are indicated by a filled square at a threshold of 370 GeV and an open square at a threshold of 260 GeV.

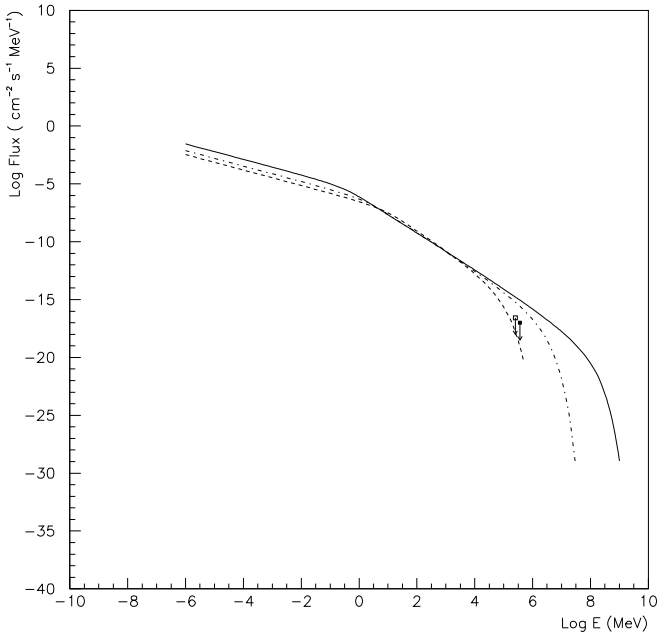

FIG. 4.—Predicted outer gap pulsed γ-ray flux from PSR B1951+32. The solid, dot-dashed, and dashed curves correspond to $\alpha = 0.5$, 0.6, and 0.7, respectively, where $\alpha = r/r_L$, is the radial distance to the synchrotron emitting region near the outer gap as a fraction of the light cylinder radius (r_L) and is a free parameter in the model (Zhang & Cheng 1997). The Whipple pulsed upper limits are shown as a filled square at a threshold of 370 GeV and an open square at a threshold of 260 GeV.

cylinder radius r_L. Our pulsed upper limits are consistent with the outer gap model if $\alpha > 0.6$ implying an emission region far out in the magnetosphere.

The result reported here is the first observation of PSR B1951+32 beyond 30 GeV. It constrains the high-energy emission of the pulsar, which rises continuously in energy output at EGRET energies. PSR B1951+32 exhibits very similar spectral behavior and morphological features, such as an associated synchrotron nebula, to PSR B1706−44 (Finley et al. 1997). If these factors are any indication of similar emission mechanisms in pulsars then the lack of unpulsed emission for PSR B1951+32 is puzzling considering that PSR B1706−44 was detected as a VHE source of unpulsed emission greater than 1 TeV (Kifune et al. 1995). Lack of pulsed emission indicates that the processes producing pulsed high-energy photons over two decades of energy in the EGRET energy range somehow become ineffective over a decade of energy to result in a lack of VHE γ rays. The low magnetic field of PSR B1951+32 relative to the average pulsar field implies that attenuation of γ rays by magnetic absorption is not a likely explanation for the nondetection. It can be concluded from observations by the EGRET detector and VHE energies reported here that pulsed emission from PSR B1951+32 cuts off between 30 GeV and 260 GeV. The pursuit of this cutoff regime will be a continuing effort of the Whipple project in the future.

We acknowledge the technical assistance of K. Harris. This research is supported by grants from the US Department of Energy and by NASA, by PPARC in the UK and by Forbairt in Ireland. The authors wish to thank A. Lyne for providing the radio ephemeris of PSR B1951+32 and D. J. Thompson for providing the multiwavelength spectrum for PSR B1951+32.

REFERENCES

Bertsch, D. L., et al. 1992, Nature, 357, 306
Biller, S., et al. 1995, in Proc. 24th Int. Cosmic-Ray Conf. (Rome), 3, 412
Catanese, M., et al. 1995, in Towards a Major Atmospheric Cherenkov Detector—IV, ed. M. Cresti (Padova), 335
Cawley, M. F., & Weekes, T. C. 1995, Exp. Astron., 6, 7
Cheng, K. S., Ho, C., & Ruderman, M. A. 1986, ApJ, 300, 500
Daugherty, J. K., & Harding, A. K. 1982, ApJ, 252, 337
Dermer, C. D., & Sturner, S. J. 1994, ApJ, 420, L75
De Jager, O. C., et al. 1995, in Proc. 24th Int. Cosmic-Ray Conf. (Rome), 2, 528
De Jager, O. C., et al. 1996, ApJ, 457, 253
Fierro, J. M. 1995, Ph.D. thesis, Stanford Univ.
Fierro, J. M., et al. 1993, ApJ, 413, L27
Finley, J. P., et al. 1997, ApJ, in preparation
Gillanders, G., et al. 1997, in Proc. 25th Int. Cosmic-Ray Conf. (South Africa), in press
Gould, R. J. 1965, Phys. Rev. Lett., 15, 577
Harding, A. K. 1997, private communication
Hillas, A. M. 1985, in Proc. 19th Int. Cosmic-Ray Conf. (La Jolla), 3, 445
Kifune, T., et al. 1995, ApJ, 438, L91
Kulkarni, S. R., et al. 1988, Nature, 331, 50
Lyne, A. G. 1996, private communication
Punch, M., et al. 1991, in Proc. 22nd Int. Cosmic-Ray Conf. (Dublin), 1991, 1, 464
Ramanamurthy, P. V., et al. 1995, ApJ, 447, L109
Romani, R. W., & Yadigaroglu, I.-A. 1995, ApJ, 438, 314
Safi-Harb, S., Ögelman, H., & Finley, J. P. 1995, ApJ, 439, 722
Srinivasan, R. 1997, Towards a Major Atmospheric Cherenkov Detector—V, South Africa, in preparation
Taylor, J. H., Manchester, R. N., & Lyne, A. G. 1993, ApJS, 88, 529
Takanori, Y. 1996, Ph.D. thesis, Univ. Tokyo
Thompson, D. J. 1996, private communication
Thompson, D. J., et al. 1992, Nature, 359, 615
Vacanti, G. 1991, ApJ, 377, 467
———. 1996, Space Sci. Rev., 75, 1
Zhang, L., & Cheng, K. S. 1997, ApJ, submitted